ACCOUNTS
—of materials research—

Open Access
This article is licensed under CC-BY 4.0

pubs.acs.org/amrcda
Article

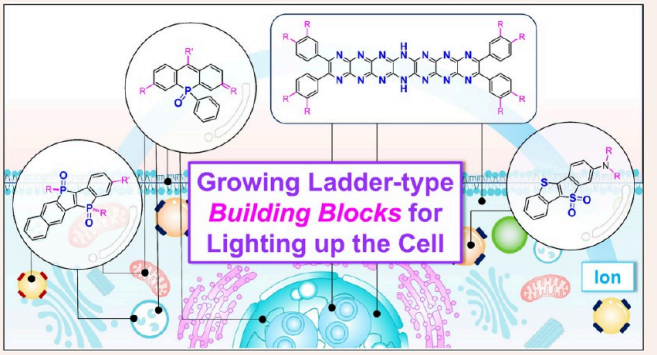
Ladder-Type π-Conjugated Heteroatom-Reinforced Nanoarchitectonics: Transformative Materials for Imaging of Cellular Components

Linawati Sutrisno, Masayasu Taki, Katsuhiko Ariga,* and Shigehiro Yamaguchi*

Cite This: *Acc. Mater. Res.* 2026, 7, 1074−1088
Read Online

ACCESS | Metrics & More | Article Recommendations | Supporting Information

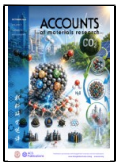
CONSPECTUS: Cell populations are inherently heterogeneous, and the molecular mechanisms that govern cellular plasticity and fate operate across broad spatial and temporal scales. Early signaling events emerge within seconds to minutes, whereas phenotypic transitions associated with differentiation, adaptation, and disease progression may unfold over hours, days, or longer. Elucidating these dynamic processes requires molecular imaging tools capable of quantitatively monitoring biochemical events with high spatial resolution, temporal precision, and molecular specificity in living systems. However, achieving this goal demands the integration of multiple design principles that are rarely realized within a single molecular platform. Therefore, the development of such tools remains a central challenge in chemical biology because molecular recognition, fluorescence signaling, organelle targeting, and photostability must be integrated within a single molecular architecture. In this Account, we present a historical overview of the evolution of our unique molecular imaging toolbox, tracing its development from *fundamental studies* of molecular recognition in artificial systems to multiplex visualization of organelle dynamics in living cells, and ultimately to their successful translation into *bioimaging probes*. Our early efforts established how *hydrogen-bonding interactions at artificial lipid membrane interfaces* can be exploited to *enhance biomolecular recognition* under aqueous conditions. These studies further revealed that tuning membrane mechanical properties provides a powerful strategy for *discriminating structurally similar nucleotide targets* and regulating selective molecular recognition. The principles derived from these artificial systems were subsequently extended to fluorescence sensing platforms for recognition of biologically relevant analytes. Building upon these molecular recognition strategies, we developed heteroatom-containing π-conjugated fluorophores in which *phosphorus, sulfur, and nitrogen elements* were strategically incorporated into *ladder-type π-conjugated compounds* to modulate electronic structure, fluorescence properties, and bioimaging performance. Systematic molecular engineering transformed these fluorophores from *intracellular ion sensors* into highly selective *organelle-targeting probes* and, ultimately, *multiplex imaging platforms* capable of simultaneously visualizing dynamic interactions among multiple subcellular compartments. Importantly, heteroatom engineering also enabled exceptional photostability, allowing long-term imaging of gradual cellular transitions that are inaccessible with conventional probes. A recurring theme throughout this work is the rational integration of molecular components to bridge chemical structure and biological function. Through precise tuning of fluorophore scaffolds, linker architectures, molecular recognition motifs, and organelle-targeting units, we established modular design principles that govern intracellular localization, selectivity, sensitivity, and imaging performance. These developments exemplify the importance of *nanoarchitectonics*, in which functional systems emerge through the hierarchical organization of atoms, molecules, supramolecular interactions, interfaces, and biomolecules. Looking forward, we envision next-generation imaging platforms that combine multiplexed sensing, adaptive functionality, and quantitative analysis to reveal the molecular basis of cellular plasticity across diverse biological systems. Such advances will provide critical spatiotemporal insights into disease onset, progression, and therapeutic response and contribute to the realization of precision medicine.



1. INTRODUCTION: CREATING THE FOUNDATION FOR INNOVATION

How do billions of biomolecules coordinate their activities within the crowded and dynamic environment of a living cell? Although these molecular interactions underpin every biological process, they remain largely invisible to the human eye. What

Received: July 4, 2026
Revised: August 22, 2026
Accepted: September 1, 2026
Published: September 22, 2026



ACS Publications
© 2026 The Authors. Co-published by ShanghaiTech University and American Chemical Society

https://doi.org/10.1021/accountsmr.6c00184
Acc. Mater. Res. 2026, 7, 1074−1088

Downloaded from pubs.acs.org/amrcda/article-pdf/7/10/1074/6859593/accountsmr.6c00184.pdf by NATL INST FOR MATLS SCIENCE (NIMS) user on 24 October 2026

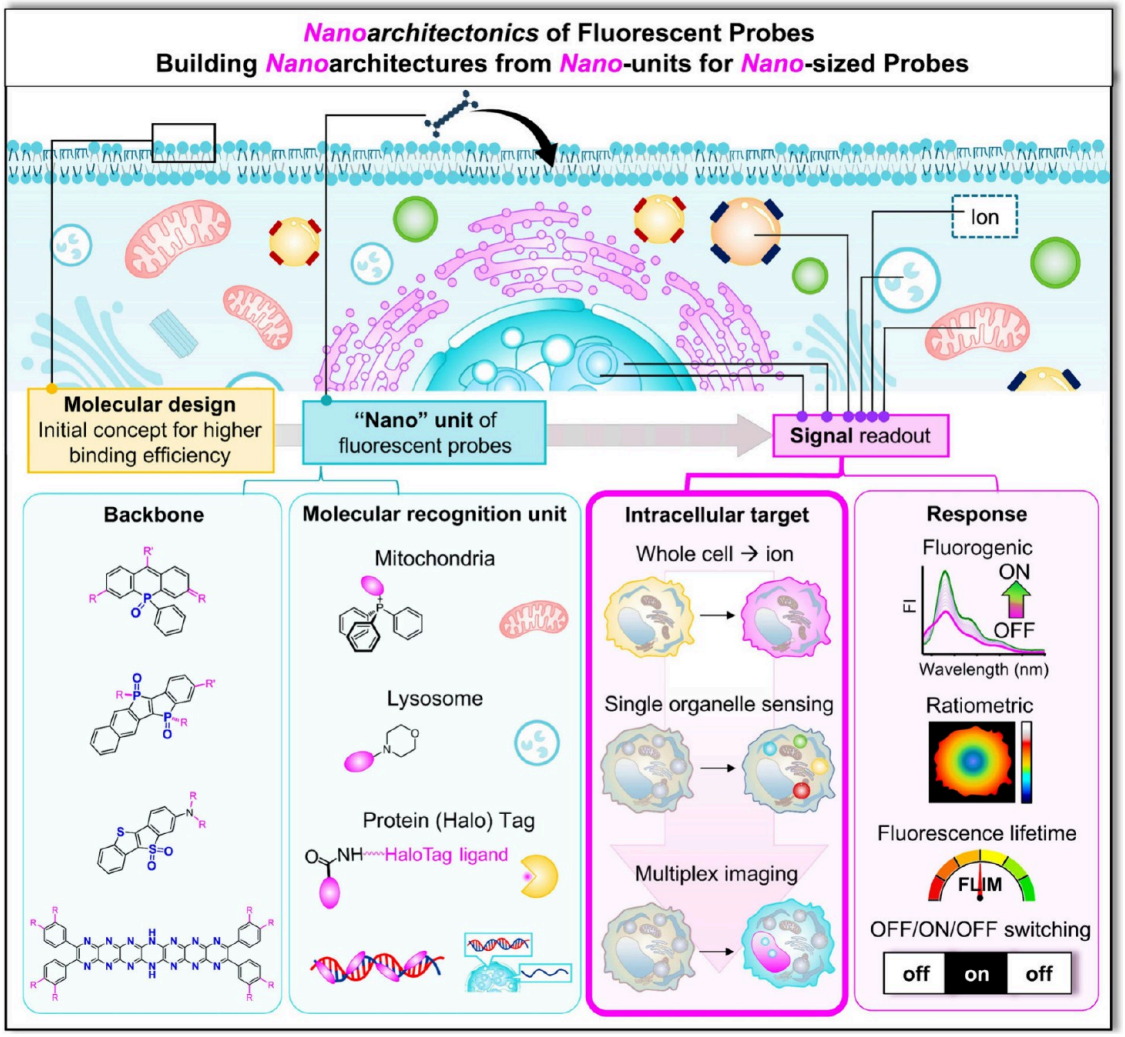


Figure 1. Nanoarchitectonics of fluorescent probe building blocks. Small-molecule probes are built from integrated nanounits, typically consisting of a backbone, a linker, and a molecular recognition motif.

would we discover if we could directly observe the molecular language of cells as it unfolds in space and time? How can we visualize these events in real time without perturbing their native functions? How can we build a molecular sensing toolbox from scratch through the rational design of innovative molecular building blocks? These questions lie at the heart of modern bioimaging research, bridging chemistry, materials science, and biology while touching upon fundamental questions about the nature of life itself.

The development of molecular imaging toolboxes is driven by the need to understand the molecular processes of life, construct de novo sensing systems, and create versatile platforms capable of revealing previously inaccessible biological phenomena.[1−3] A central challenge is the design of imaging agents that integrate high target affinity, efficient molecular recognition, excellent photostability, and operational simplicity in complex biological environments. Fulfilling these demands requires not only the refinement of existing molecular nanoarchitectures but also the continuous growth of molecular building blocks.[4−7] Therefore, there is an urgent need for small-molecule fluorescent probes that can be readily applied to living systems to report intracellular dynamic changes over time.

While previous reviews have highlighted specific aspects of our research development in fragmented contexts,[8−15] a comprehensive account of our research roadmap has not yet been presented. In contrast to our recent review, which focused on molecular probe nanoarchitectonics for RNA/DNA imaging, this Account covers the broader development of heteroatom-containing ladder-type π-conjugated fluorophores for ion sensing, organelle imaging, super-resolution imaging, and multiplex cellular imaging.[10] In this Account, we outline the progression of our molecular design philosophy, from early molecular recognition in artificial biological systems (Figure 1 and Figure 2) to the development of ion-sensing and organelle targeting probes. Here, nanoarchitectonics refers to the hierarchical integration of heteroatom-containing π-conjugated scaffolds, recognition motifs, linker architectures, targeting groups, and biological interfaces to produce emergent imaging functions (Supplementary Figure S1). Then, we describe the structural evolution of imaging platforms through phosphorus-, sulfur-, and nitrogen-containing π-conjugated scaffolds. Finally, we discuss future directions, remaining challenges, and how nanoarchitectonic can guide the development of next-generation imaging platforms for visualizing dynamic cellular processes.

Downloaded from pubs.acs.org/amrcda/article-pdf/7/10/1074/6859593/accountsmr.6c00184.pdf by NATL INST FOR MATLS SCIENCE (NIMS) user on 24 October 2026

https://doi.org/10.1021/accountsmr.6c00184
Acc. Mater. Res. 2026, 7, 1074−1088

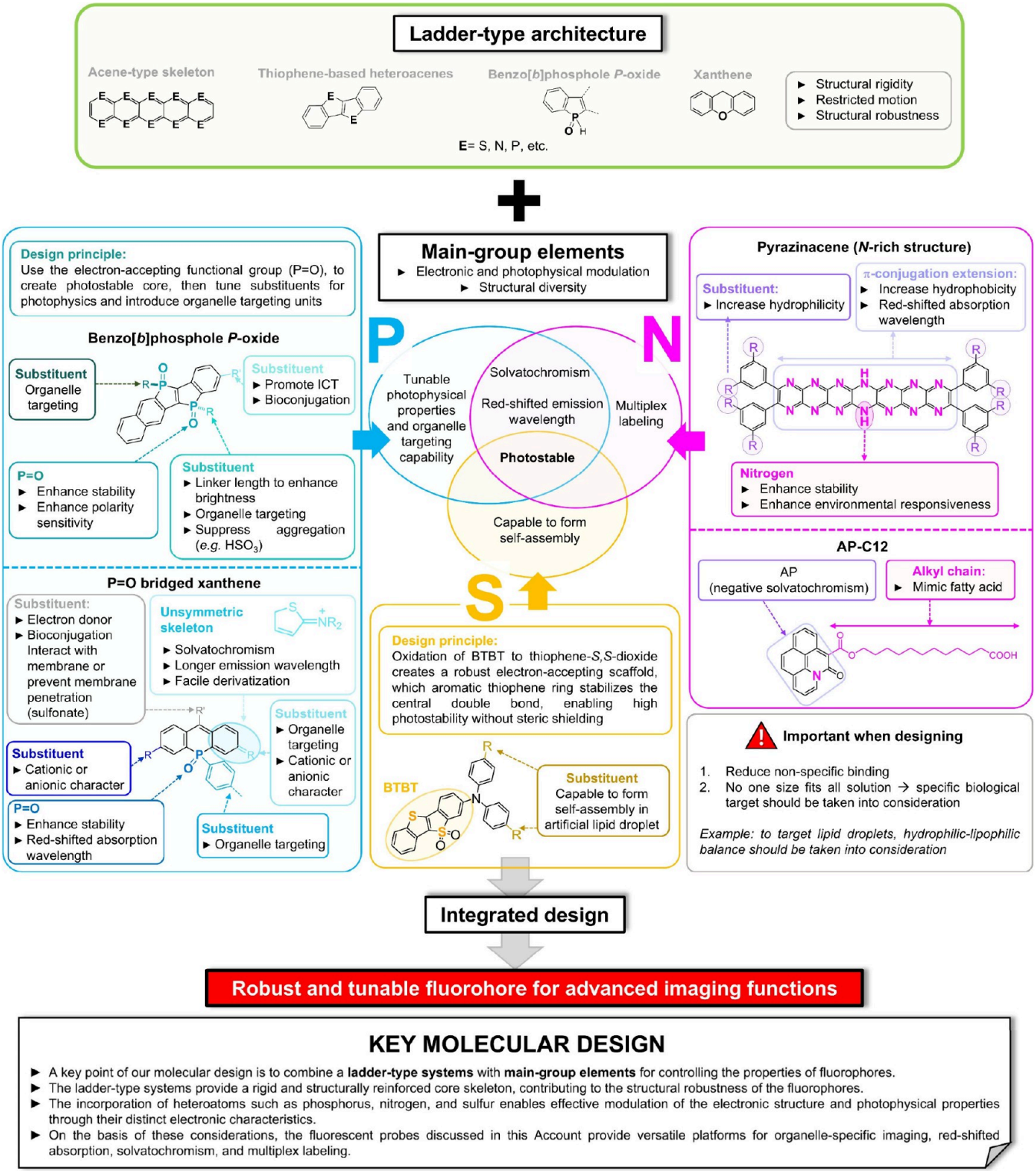


Figure 2. General molecular design strategies based on heteroatom incorporation discussed in this Account.

2. EARLY CURIOSITY: A KEY TO ENHANCE BIOMOLECULAR RECOGNITION

Our research journey into bioimaging was initiated by an early curiosity to examine the binding efficiency of different biomolecules in artificial lipid membranes (Figure 3A). Using Langmuir monolayers at the air−water interface as models of cell membrane surfaces, we demonstrated that biomolecules can be effectively recognized through hydrogen bonding even in aqueous environments.[16,17] A guanidinium−phosphate model system showed that binding constants increase from 1.4 M^{-1} in bulk water to 10^6−10^7 M^{-1} at the air−water interface, highlighting the unusual enhancement of molecular recognition at biological interfaces. Building on this concept, we further achieved discrimination of uracil over thymine using a mechanically tuned triazacyclononane monolayer and developed a mechanically controlled indicator displacement assay

https://doi.org/10.1021/accountsmr.6c00184
Acc. Mater. Res. 2026, 7, 1074−1088

Downloaded from pubs.acs.org/amrcda/article-pdf/7/10/1074/6859593/accountsmr.6c00184.pdf by NATL INST FOR MATLS SCIENCE (NIMS) user on 24 October 2026

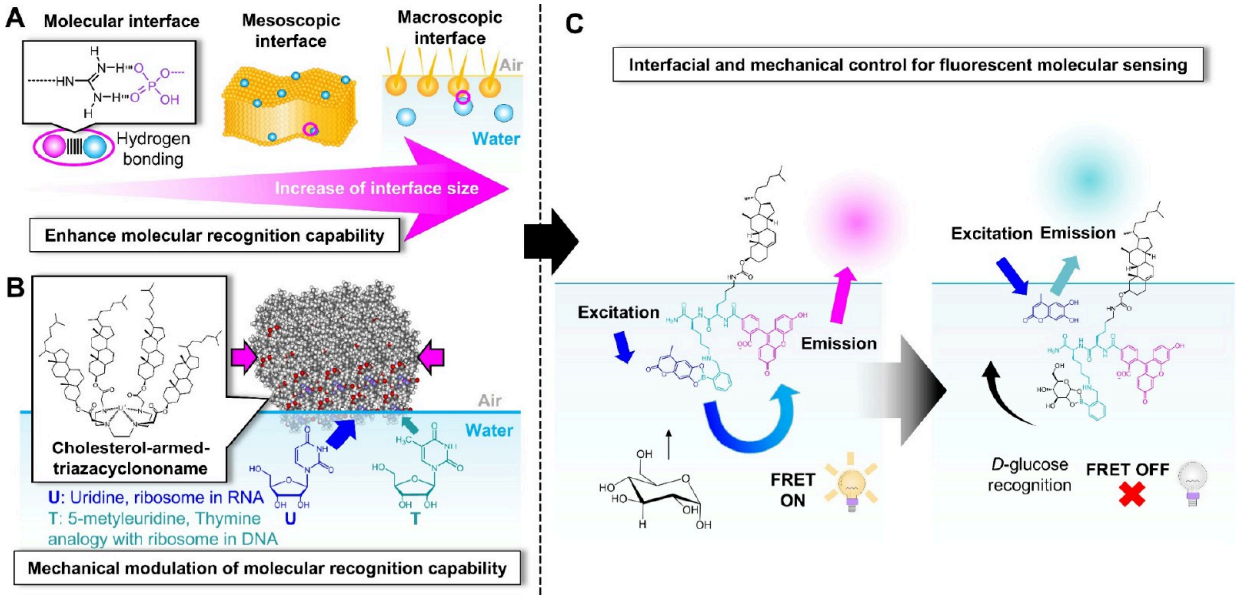


Figure 3. Biomolecular recognition in artificial biological systems. (A) Enhanced molecular recognition through expansion of the interfacial area. (B) Mechanical modulation enables RNA/DNA discrimination in a biomimetic system. (C) Interfacial and mechanical regulation of fluorescent molecular recognition for *D*-glucose sensing.

(MC-IDA) for highly sensitive fluorescence sensing (Figure 3B and Figure 3C).[18] This pioneering research was instrumental in guiding our rational design of fluorescent probes through intramolecular hydrogen-bonding interactions.[19] In particular, insights gained from these studies established an early experimental foundation that integrates the roles of heteroatom incorporation, molecular recognition, electronic modulation, environmental responsiveness, and subcellular localization within a nanoarchitectonic framework. Building on this nanoarchitectonic principle, we developed a series of fluorescent probes, beginning with metal-ion detection and expanding to single-organelle and multiplexed organelle imaging.

3. WHOLE-CELL IMAGING OF INTRACELLULAR IONS

Fluorescent chemosensors have become useful tools for quantitative measurements of intracellular changes in metal ion concentration due to their high optical sensitivity and spatial resolution. Early examples of small-molecule ion sensors include quinoline-, fluorescein-, benzazole-, and coumarin-based probes. They generally suffer from small Stokes shifts, substantial fluorescence enhancement or quenching upon Zn^{2+} binding, or insufficient affinity for Zn^{2+}. To overcome these limitations, we developed a fluorescent zinc reporter (**1**), derived from the Zinbo family of probes based on a highly emissive benzoxazole scaffold functionalized with various Zn^{2+}-chelating groups (Figure 4A).[20] Compound (**1**) showed a pZn value of 9.3, comparable to Zinquin, Zinpyr, and ZnAF probes, and significantly higher Zn^{2+} affinity than DPA, likely due to additional coordination by the phenolate oxygen and benzoxazole nitrogen atoms. Among physiologically relevant metal ions, Zn^{2+} and Cd^{2+} often interfere with each other in fluorescence imaging, while Mn^{2+}, Co^{2+}, Ni^{2+}, Fe^{2+}, and Cu^{2+} quench the fluorescence. To improve Zn^{2+} selectivity and affinity, we further synthesized ZID-1 (**2**) based on an intramolecular charge transfer (ICT) mechanism using a 2-(4-aminophenyl) indole fluorophore.[21] A pyridylmethyl arm was introduced through an oxygen linker positioned *ortho*-position of the amino group to enhance metal coordination. The photophysical properties of (**2**) suggest that the incorporated pyridyl group acts as the fourth ligand for Zn^{2+} coordination, resulting in a suitable binding affinity (K_d = 17.1 nM) for intracellular zinc imaging. We subsequently designed the Cd^{2+}-selective fluorescent sensor CadMQ (**3**), which showed excellent selectivity for Cd^{2+} over other transition metal ions, including Zn^{2+}, in aqueous media, with a detection limit below 100 pM for monitoring Cd-induced biological processes, while also enabling dual-excitation ratiometric Cd^{2+} imaging (Figure 4B).[22]

Since Cu(I) is the predominant oxidation state in the reducing cytosolic environment, Cu(I)-selective probes with fluorescence turn-on responses are particularly desirable for cellular imaging. However, many reported Cu(I) chemosensors suffer from limitations such as fluorescence quenching, high background signals, and the requirement for precise concentrations of two interacting components to generate fluorescence enhancement. To address this challenge, we synthesized the copper-selective fluorescent probe FluTPA2 (**4**) (Figure 4C).[23] The hydrophobic character of (**4**) enhances cell membrane permeability, allowing efficient intracellular detection of Cu^{+}. Upon reaction with intracellular Cu^{+}, (**4**) undergoes Cu^{+}-mediated C−O bond cleavage followed by air oxidation to generate a highly fluorescent xanthene dye in living cells. Although (**4**) successfully enabled imaging of intracellular Cu^{+} in living cells, diffusion of both the probe and its fluorescent product into the cytosol prevented selective visualization of organelle-stored Cu^{+}. We therefore designed a spirocyclized rhodol-based fluorescent probe (**5**) for the selective detection of mitochondrial Cu^{+}.[24] Alkylation of the xanthene hydroxy group with a tris(2-pyridylmethyl) amine-derived ligand generated a nonfluorescent spirocyclic form, while reaction with Cu^{+} in the presence of submillimolar glutathione at physiological pH triggered ligand cleavage and fluorescence activation of the rhodol scaffold. This probe enabled visualization of mitochondrial Cu^{+} in copper-supplemented cells.

Another attractive approach for monitoring ion sensing is the development of switchable Hg^{2+} sensors (Figure 4D).[25] In

https://doi.org/10.1021/accountsmr.6c00184
Acc. Mater. Res. 2026, 7, 1074−1088

Downloaded from pubs.acs.org/amrcda/article-pdf/7/10/1074/6859593/accountsmr.6c00184.pdf by NATL INST FOR MATLS SCIENCE (NIMS) user on 24 October 2026

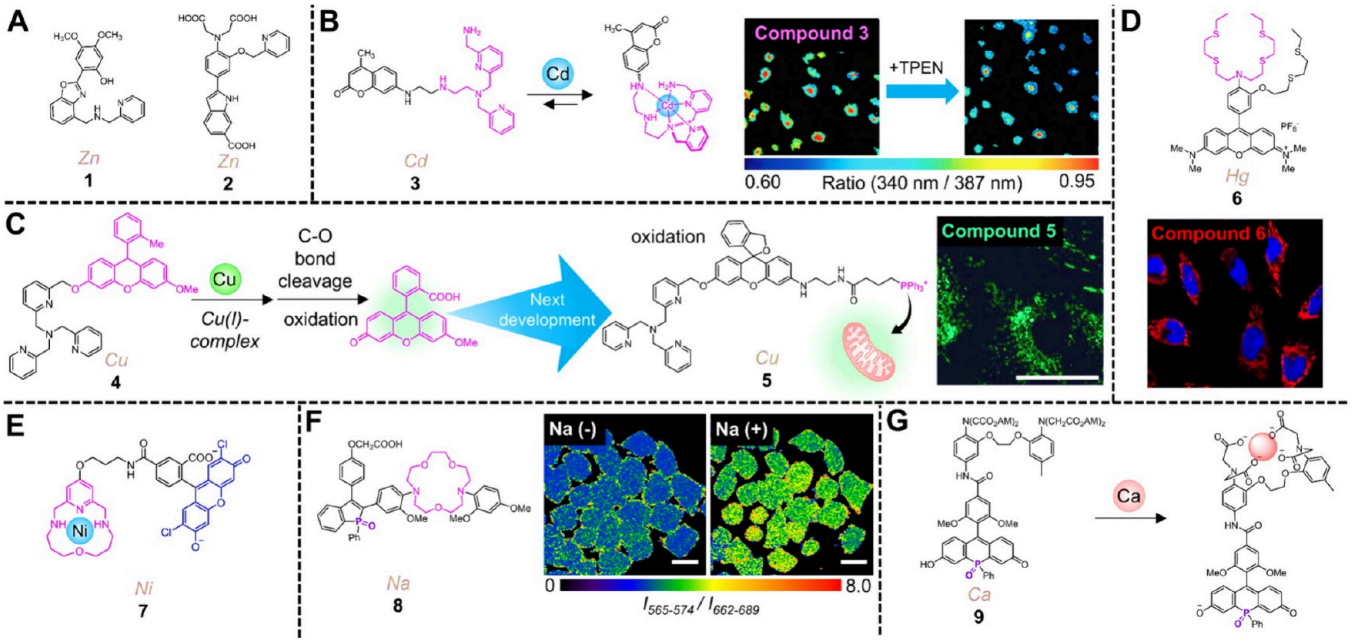


Figure 4. Historical development of ion-sensing probes developed by our group. (A) Chemical structure of Zn-fluorescent probes (**1**–**2**). (B) Cd-responsive ratiometric fluorescent probe (**3**) designed with a tailored chelating recognition interface. Reproduced with permission from Ref 22. Copyright 2008, American Chemical Society. (C) Cu-targeting fluorescent probe (**4**–**5**). TPEN, *N,N,N′,N′*-tetrakis(2-pyridylmethyl) ethylenediamine. Scale bar: 50 μm. Reproduced with permission from Ref 24. Copyright 2014, The Royal Society of Chemistry. (D) Hg-selective fluorescent probe **6** based on sulfur-rich molecular recognition architecture. Scale bar: 50 μm. Reproduced with permission from Ref 25. Copyright 2012, American Chemical Society. (E) Chemical structure of NiL^{O}DCF (**7**). (F) Na-responsive fluorescent probe (**8**) incorporating a crown ether-based molecular recognition unit for intracellular Na imaging. Reproduced with permission from Ref 28. Copyright 2015, The Royal Society of Chemistry. Scale bar: 20 μm. (G) Ca-selective probe (**9**) consists of a molecular recognition site for fluorescence activation upon Ca binding.

general, Hg^{2+} binding induces fluorescence quenching through the heavy-atom effect, and most reported Hg^{2+} sensors rely on irreversible oxymercuration or desulfurization reactions. However, these systems are often unsuitable for real-time intracellular imaging and cannot reversibly monitor changes in free Hg^{2+} levels. Therefore, we designed RosHg (**6**) based on a rosamine scaffold for selective Hg^{2+} detection. Compound (**6**) showed an approximately 20-fold enhancement in fluorescence upon Hg^{2+} binding, while the fluorescence rapidly decreased after addition of glutathione to the Hg–RosHg complex. The Hg^{2+} binding affinity was extremely high, with a dissociation constant of 0.10 fM determined using Hg^{2+}/Mg^{2+}/EDTA buffer systems. Confocal fluorescence imaging further demonstrated that **6** can monitor dynamic changes in mitochondrial Hg^{2+} levels in living cells. Another elegant example of a switchable fluorescent probe is NiL^{O}DCF (**7**), which we synthesized based on the fluorophore displacement mechanism (Figure 4E).[26] A macrocyclic nickel(II) complex (NiL^{O}) conjugated with dichlorofluorescein (DCF) was developed as a fluorescent probe for His-tag recognition. Coordination of the DCF phenolic oxygen to NiL^{O} caused fluorescence quenching, while binding of a hexahistidine peptide induced strong fluorescence enhancement through formation of a 1:1 ternary complex. Compound (**7**) showed effective recognition of polyhistidine sequences with dissociation constant of 24 ± 1 AμM, demonstrating potential application as a reversible fluorescent sensor for His-tagged proteins.

Improved detection limits and sensitivity in ion sensing can be achieved using π-conjugated D–π–A fluorophores composed of electron-donating (D) and electron-accepting (A) moieties, which exhibit emission from an ICT excited state. Upon interaction of the donor moiety with a target metal ion, the ICT character is reduced, resulting in hypsochromic shifts in both the absorption and emission spectra. Based on this strategy, we previously developed a D–π–A fluorophore incorporating triphenylamine as the electron donor and benzo[*b*]phosphole *P*-oxide as the electron acceptor.[27] This fluorophore exhibited strong polarity-dependent fluorescence changes together with excellent photostability, making benzophosphole oxide a promising skeleton for long-term metal ion tracking in living systems. Using the D–π–A-type benzophosphole *P*-oxide framework, we also developed a membrane-permeable ratiometric sodium probe, NaGY (**8**), by incorporating a diazacrown ether moiety that functions both as a sodium ion-binding site and an electron-donating group (Figure 4F).[28]

To extend this strategy to long-wavelength imaging, we developed cytosolic calcium imaging probes based on the far-red-emitting fluorescein analogue phospha-fluorescein (PF) (**9**), which contains a phosphine oxide (P═O) moiety at the 10-position of the fluorescein scaffold (Figure 4G).[29] Owing to its low-lying LUMO induced by the electron-withdrawing phosphine oxide moiety and a narrow HOMO–LUMO gap from effective σ^*–π^* conjugation, PF shows red-shifted absorption (λ_{abs} = 627 nm) and emission (λ_{em} = 656 nm) in neutral aqueous buffer. The hydrophilic and anionic nature of this phospha-fluorescein fluorophore enabled cytosolic localization of probe (**9**) and allowed visualization of histamine-induced calcium oscillations in HeLa cells. Encouraged by these findings, we have extended our research toward the design and functionalization of ladder-type π-conjugated frameworks containing phosphorus, nitrogen, and sulfur to create fluorescent probes with improved photostability, prolonged imaging capability, and precise subcellular localization.

https://doi.org/10.1021/accountsmr.6c00184
Acc. Mater. Res. 2026, 7, 1074–1088

Downloaded from pubs.acs.org/amrcda/article-pdf/7/10/1074/6859593/accountsmr.6c00184.pdf by NATL INST FOR MATLS SCIENCE (NIMS) user on 24 October 2026

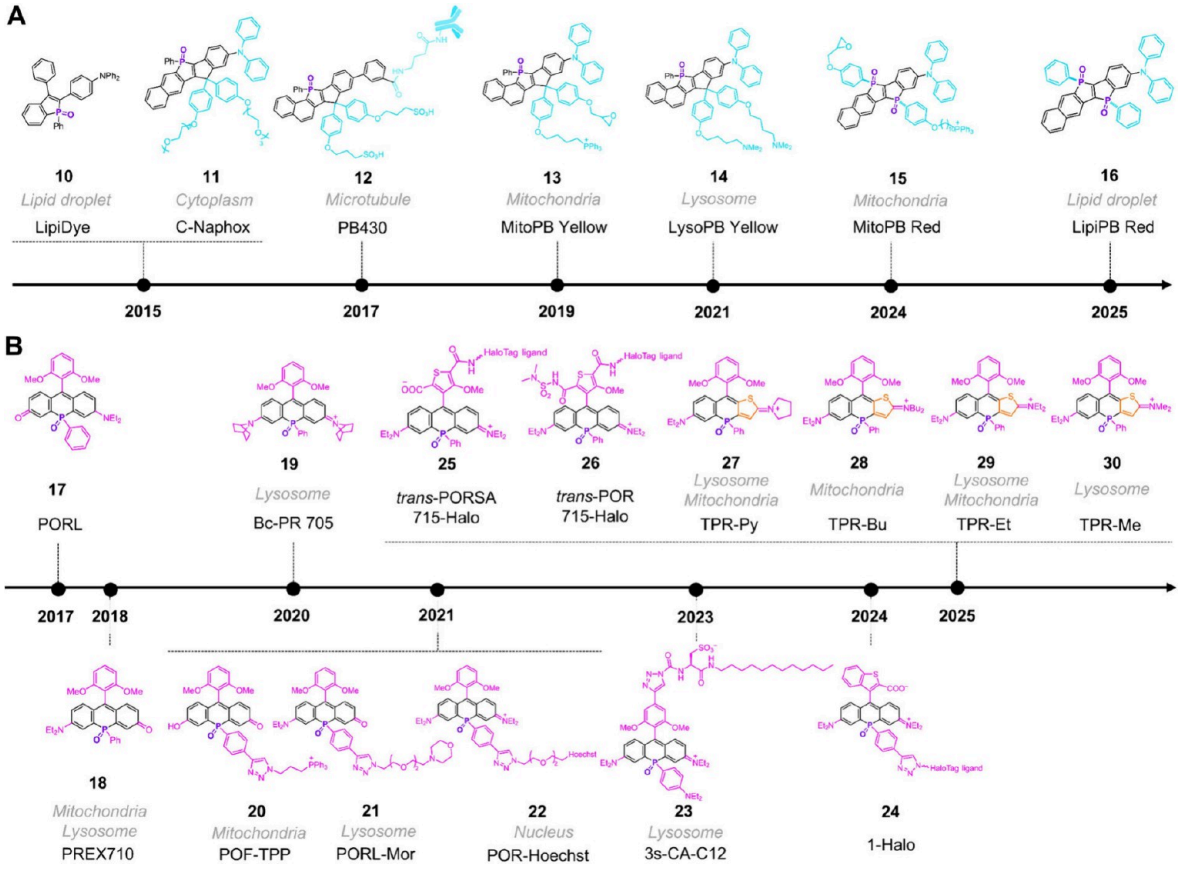


Figure 5. Timeline for the emergence of phosphole-oxide probes. (A) Milestones in the development of benzo[*b*]phosphole *P*-oxide probes (**10**-**16**). (B) Milestones in the design of P═O-bridged xanthene probes (**17**-**30**).

4. SINGLE-ORGANELLE MONITORING WITH FLUORESCENT PROBES

Extending beyond ion sensing, we further explored the application of our phosphole-oxide probes for organelle-specific imaging (Figure 5). In particular, our interest in phosphole oxide systems stems from their highly electron-accepting character, which renders them versatile platforms for the development of photostable fluorophores and intracellular sensing probes. In this section, we highlight the development of phosphole oxide-based fluorescent probes for single-organelle imaging applications.

4.1. Benzo[*b*]phosphole *P*-oxide

Environment-sensitive fluorescent probes are important for visualizing changes associated with cellular events, and several fluorophores such as Prodan, 1,8-ANS, dapoxyl, and Nile red have been reported. Compared with these systems, the D−π−A-type benzo[*b*]phosphole *P*-oxide (**10**) offers several advantages, including compatibility with commonly used 405 nm LED excitation in fluorescence microscopy and red emission (Figure 6A).[27] These features prompted us to investigate compound (**10**) as a potential fluorescence probe. Briefly, electron-donating aryl groups were incorporated into electron-accepting benzo[*b*]phosphole scaffolds to generate a series of donor−π−acceptor fluorophores. One of benzo[*b*]phosphole *P*-oxide derivative (**10**) maintained high fluorescence quantum yield even in polar protic solvents and exhibited obvious solvent-dependent emission shifts with minimal changes in absorption. These properties enabled its application in adipocyte staining, where subcellular polarity differences could be distinguished via emission color variation. In differentiated 3T3−L1 adipocytes stained with (**10**), the emission maximum was observed at 521 nm, whereas other intracellular regions showed a red-shifted emission maximum at 565 nm. Using these two spectral properties, the image was unmixed, and the fluorescent solvatochromism of (**10**) allowed us to visualize intracellular lipids up to 8 days. Next, we designed a structurally reinforced derivative of (**10**) for high-resolution STED imaging with reduced photobleaching, which was denoted as C-Naphox (**11**).[30] Compound (**11**) was rationally designed by combining an electron-accepting phosphole *P*-oxide unit with an electron-donating triphenylamine moiety and further reinforcing the naphthophosphole scaffold through carbon-bridge incorporation, which was designed based on three key considerations: (i) enhanced fluorescence intensity, molar absorption coefficient, and quantum yield in polar and protic media arising from the carbon-bridged and naphthalene-fused structure; (ii) ICT-induced large Stokes shifts that minimize self-absorption and anti-Stokes excitation under STED conditions; and (iii) pronounced solvatochromic emission shifts with increasing solvent polarity. Accordingly, compound (**11**) retained 99.5% of its fluorescence intensity even after irradiation with a Xe lamp (300 W, λ_{ex} = 460 nm, FWHM = 11 nm) and continuous 405 nm laser exposure for 2 h, likely due to protection of the central double bond by the phosphoryl group and carbon bridge against photooxidative degradation.

Using a similar approach, PB430 (**12**) was developed by replacing the amino group of (**11**) with an aryl group, thereby converting the excited-state character from ICT to a π−π* transition, enabling intense fluorescence even in aqueous

https://doi.org/10.1021/accountsmr.6c00184
Acc. Mater. Res. 2026, 7, 1074−1088

Downloaded from pubs.acs.org/amrcda/article-pdf/7/10/1074/6859593/accountsmr.6c00184.pdf by NATL INST FOR MATLS SCIENCE (NIMS) user on 24 October 2026

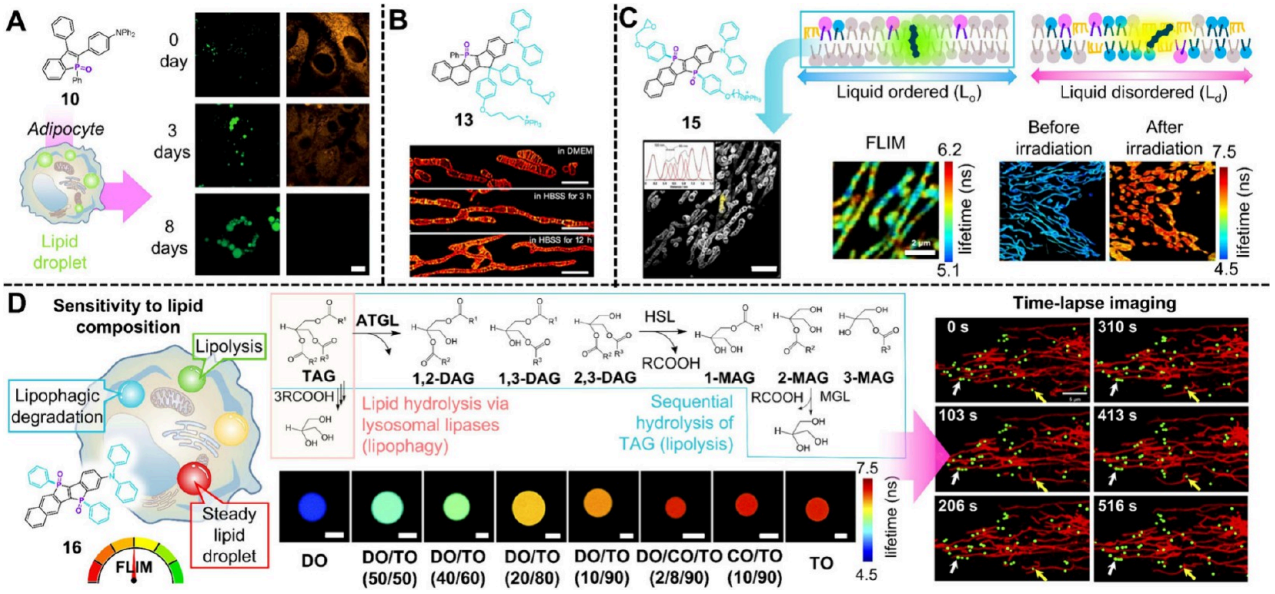


Figure 6. Representative sensing of various P═O fluorescent probes. (A) Representative confocal image of adipocyte-stained with LipiDye (**10**). The confocal images were taken in the range of λ_{ex} = 405 nm and λ_{em} = 521−530 nm and λ_{em} = 556−565 nm is shown in green (left) and orange (right), respectively. Scale bar: 10 μm. Reproduced with permission from Ref 27. Copyright 2015, Wiley-VCH. (B) Chemical structures of C-Naphox (**11**) and its modified analogue MitoPB Yellow (**13**). Deconvolved STED micrographs reveal changes in mitochondrial structure together with alterations in cristae density after staining with (**13**) upon 3- and 12-hour nutritional starvation in Ca^{2+}- and Mg^{2+}-containing HBSS (λ_{ex} = 488 nm; λ_{STED} = 660 nm, bottom images). Scale bar: 2 μm. Reproduced with permission from Ref 32. Copyright 2015, PNAS, licensed under CC BY 4.0. (C) Mechanism underlying membrane order sensing by MitoPB Red (**15**). In less polar and more ordered domains predominantly formed by saturated phospholipids, this probe displays a longer fluorescence lifetime. By contrast, shorter fluorescence lifetimes are detected in more hydrated or disordered lipid environments rich in unsaturated phospholipids such as cardiolipin. Scale bar: 2 μm. Reproduced with permission from Ref 34. Copyright 2024, Wiley-VCH, licensed under CC BY 3.0. (D) Sensitivity of LipiPB Red (**16**) to lipid compositions characterized via FLIM (left) and long-term imaging results (right). Scale bar: 5 μm. Reproduced with permission from Ref 35. Copyright 2025, American Chemical Society.

media.[31] Furthermore, removal of the electron-donating diphenylamino group induced a blue shift of the absorption band into the UV region. To recover visible-light excitation capability, we altered the fusion mode of the naphthalene moiety in (**12**), which red-shifted the absorption band with an absorption edge extending to 480 nm, thereby enabling excitation with a 470 nm laser commonly employed in STED microscopy. Compound (**12**) also contains a bioconjugatable functional group that enables antibody labeling through NHS ester formation. The resulting (**12**)-conjugated antibodies exhibited exceptional photostability, allowing repeated STED imaging without antifading agents, while retaining over 50% fluorescence intensity after 30 image acquisitions. Another similar approach involved the development of MitoPB Yellow (**13**), which was designed for STED imaging of mitochondrial membrane dynamics based on compound (**11**), a fluorophore comprising a naphthophosphole *P*-oxide scaffold and an electron-donating triphenylamine moiety (Figure 6B).[32] Due to ICT character of (**11**), which resulted in diminished fluorescence in aqueous media (*i.e.* mitochondrial or lysosomal matrix) but bright emission in nonpolar environments (*i.e.* lipid bilayer membranes), we envisioned that this property would enable high-contrast visualization of lipid membranes. To optimize mitochondrial labeling, we employed a naphthalene-1,2-diyl−fused phosphole *P*-oxide core to achieve longer-wavelength absorption and emission as well as further introduced a lipophilic triphenylphosphonium cation and a reactive epoxide group for selective and stable labeling of mitochondrial membranes through covalent attachment to proximal membrane proteins. As expected, the long fluorescence lifetime (approximately 8 ns) and exceptional photostability of this fluorophore enabled STED imaging of mitochondrial inner membrane (45 ± 5 nm) with a resolution of approximately 60 nm using 660 nm depletion. The probe provided detailed morphological information on cristae architecture and allowed visualization of dynamic ultrastructural processes. Based on the exceptional photostability of (**13**), we developed an analogue with enhanced lysosomal selectivity by introducing a dimethylamino group into the side chain, yielding LysoPB Yellow (**14**).[33] In addition, the phosphole oxide scaffold increases the hydrophilicity of the probe, thereby reducing nonspecific interactions and improving lysosomal targeting. Despite this increased hydrophilicity, the fluorophore core of (**14**) remains sufficiently hydrophobic to preferentially partition into the lysosomal lipid bilayer, where it emits intense yellow fluorescence. In contrast, although a fraction of the probe is also present in the hydrophilic lysosomal matrix, its fluorescence is largely quenched because the highly polar environment lowers the fluorescence quantum yield due to ICT character of fluorophore skeleton. As a result, (**14**) enables clear visualization of lysosomal membrane structures in living cells with a spatial resolution of up to 70 nm.

The limited sensitivity of the mono-P═O fluorophores (**10**−**14**) to nonpolar environmental changes limited their application in probing membrane dynamics. To address this limitation, we developed a red-emissive inner mitochondrial membrane (IMM) marker featuring a phospholo[3,2-*b*]phosphole *P*,*P*′-dioxide (bis-P═O) core with diverse arene-fused substructures, which was denoted as MitoPB Red (**15**) (Figure 6C).[34] In particular, bis-P═O dyes possess a larger excited-state dipole moment than their mono-P═O counterparts, leading to stronger interactions with surrounding solvent molecules. As

https://doi.org/10.1021/accountsmr.6c00184
Acc. Mater. Res. 2026, 7, 1074−1088

Downloaded from pubs.acs.org/amrcda/article-pdf/7/10/1074/6859593/accountsmr.6c00184.pdf by NATL INST FOR MATLS SCIENCE (NIMS) user on 24 October 2026

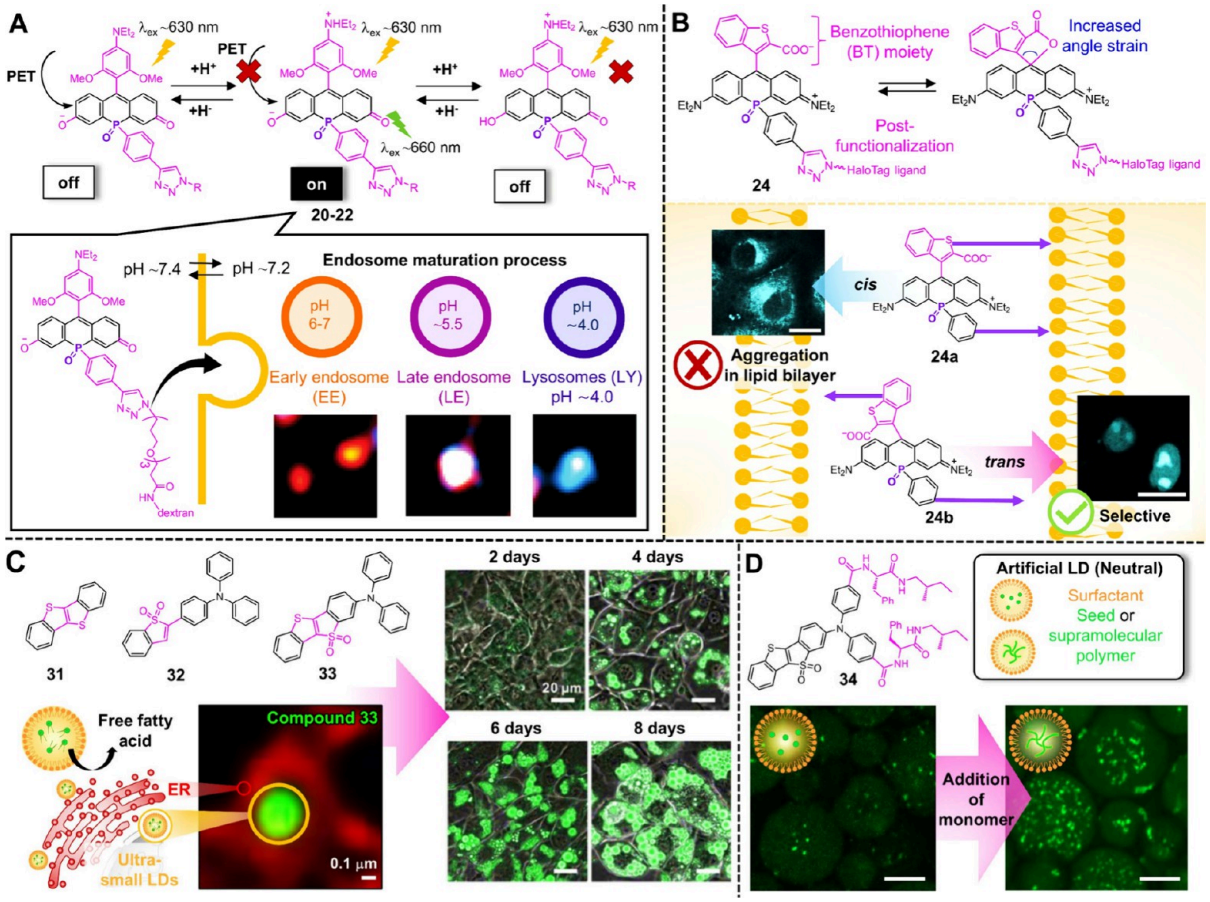


Figure 7. Representative examples of long-term imaging probes. (A) Fluorescent protonated states of Et_2NPOF (**20-22**) under 630 nm (left) and 480 nm (right) excitation. Endosomal fluorescence imaging of HeLa cells treated with Et_2NPOF-dex conjugate (bottom). Reproduced with permission from Ref 40. Copyright 2021, The Royal Society of Chemistry, licensed under CC BY 3.0. (B) Stereochemistry-dependent organelle labeling. The *cis* isomer (**24a**) exhibited non-specific accumulation on organelle membranes, while the *trans* isomer (**24b**) achieved selective labeling of HaloTag-fused proteins. Acquisition conditions for (**24**) are λ_{ex} = 730 nm, λ_{em} = 749−790 nm) Reproduced with permission from Ref 42. Copyright 2024, Wiley-VCH. Scale bar = 50 μm. (C) Rational design of super-photostable dyes: BTBT (**31**) as a fully ring-fused scaffold, chemical structure of LAQ1 (**32**), chemical structure of a partially ring-fused benzothiophene, BTO (**33**). Scale bar: 0.1 μm. Acquisition conditions for (**32**):λ_{ex} = 473 nm, λ_{em} = 490−540 nm. Reproduced with permission from Ref 45. Copyright 2021, American Chemical Society. (D) Confocal microscopy images of LAQ1 derivative (**34**) showing monomers and aggregates within an artificial lipid droplet after 210 s vortexing and 2 h incubation (λ_{ex} = 405 nm, λ_{em} = 470−540 nm). Scale bar = 30 μm. Reproduced with permission from Ref 46. Copyright 2026, Wiley-VCH.

solvent polarity increases, the ICT state becomes increasingly stabilized, promoting non-radiative decay and shortening the fluorescence lifetime. This enhanced electron-accepting character results in significantly greater sensitivity to environmental polarity. Moreover, incorporation of a second phosphoryl group also induces bathochromic shifts in absorption and emission, enabling efficient 775 nm STED depletion, while simultaneously improving photostability and polarity sensitivity. These properties enabled the use of (**15**) for both STED imaging of mitochondrial cristae and fluorescence lifetime imaging microscopy (FLIM) analysis of lipid heterogeneity within the IMM. Using this probe, we revealed that oxidative stress induces lifetime changes consistent with decreased local polarity and increased membrane order during mitochondrial remodeling and further demonstrated nanoscale differences in lipid order between the inner boundary and crista membranes. The high polarity sensitivity of (**15**) prompted us to further explore phosphole oxide-based probes for FLIM analysis of LD dynamics.[35] Recently, we developed LipiPB Red (**16**) to investigate LD heterogeneity and to track lipophagy processes. To achieve selective partitioning into LD and long-term retention, all alkyl substituents were removed from the core structure of (**16**), thereby minimizing nonspecific accumulation in organelle membranes (Figure 6D). A key aspect of this design is the balance between hydrophobicity and aqueous dispersibility, which suppresses aggregation in incubation media while promoting efficient delivery and selective accumulation within the neutral lipid-rich core of LDs. Although (**16**) is a neutral molecule with a high log P value, aggregation in aqueous environments is minimized by the highly polarized bis-P═O scaffold, overcoming a common limitation of hydrophobic fluorophores. Owing to its exceptional polarity sensitivity, (**16**) is particularly well suited for FLIM, enabling visualization of lifetime differences associated with triacylglycerol (TAG)- and diacylglycerol (DAG)-rich lipid environments within individual LDs during long-term imaging. Using this approach, we demonstrated that DAG accumulation precedes LD shrinkage during lipolysis and further revealed that lipid hydrolysis occurs before autophagosome−lysosome fusion during lipophagy.

4.2. P═O-Bridged Xanthene

Previously, one of our laboratories developed a series of *P*-fluoresceins containing phenylphosphine oxide (>P(O)Ph)

https://doi.org/10.1021/accountsmr.6c00184
Acc. Mater. Res. 2026, 7, 1074−1088

Downloaded from pubs.acs.org/amrcda/article-pdf/7/10/1074/6859593/accountsmr.6c00184.pdf by NATL INST FOR MATLS SCIENCE (NIMS) user on 24 October 2026

bridging groups, which exhibited markedly red-shifted fluorescence and high fluorescence quantum yields in water compared with fluorescein.[36] In addition, their photostability was dramatically enhanced because of the lower highest occupied molecular orbital (HOMO) energy levels. We subsequently developed previously unknown P═O-bridged rhodols (PORLs), which can be efficiently synthesized through the hydrolysis of phosphorus-substituted rhodamine probes (PORs) under basic aqueous conditions.[37] As expected, PORL (**17**) exhibits pronounced solvatochromic absorption and intense near-infrared fluorescence in aqueous media. Both PORs and PORLs show remarkable photostability, surpassing that of their oxygen- and silicon-substituted counterparts. Building on these works, we further developed PORs (**18**) upon substitution at the 9-position with a 2,6-dimethoxyphenyl group.[38] Compound (**18**) enabled long-term and three-color vis-NIR imaging of mitochondria in living cells. Owing to its high photostability, (**18**) also allowed single-molecule tracking under physiological conditions, while its dextran conjugate enabled deep imaging of mouse brain blood vessels.

Inspired by previous studies showing that cyclic or bicyclic amino groups improve the photostability of rhodamine analogues, we wondered whether amino group substitution might affect photophysical properties of phosphorus-bridged rhodamines (*P*-rhodamines).[39−41] To this end, a series of *P*-rhodamines bearing acyclic and cyclic amines, including dimethylamine, diethylamine, azetidine, pyrrolidine, and 7-azabicyclo[2.2.1]heptane (7ABH), was synthesized. Among them, the 7ABH-substituted dye (**19**) exhibited enhanced NIR fluorescence and enabled pH-independent lysosomal imaging in live cells. Furthermore, ring fusion of the amine moieties caused significant red shifts, giving absorption and emission maxima at 770 and 820 nm, respectively.

Despite their superior photostability, *P*-xanthene (POX) dyes share with conventional xanthene fluorophores a restricted number of sites for chemical modification, mainly at the 9-aryl position and the O/N termini.[42] To overcome these drawbacks, we developed NIR POX probes (**20**−**22**) bearing a 4-ethynylphenyl substituent on the phosphorus atom. The terminal alkyne enables late-stage copper-catalyzed azido-alkyne cycloaddition (CuAAC) conjugation with azide-containing molecules without altering the photophysical properties, allowing selective staining of various organelles, including mitochondria, lysosomes, and cell nuclei (Figure 7A). Functionalization of the phospha-fluorescein (POF) scaffold with the high-molecular-weight biomolecule amino dextran, combined with the design of an "off−on−off" pH-sensing mechanism, enabled the development of a dual-switching probe for visualizing endosomal maturation. Although modification of PORs is valuable, synthesis of their precursor is low-yielding, and generates difficult-to-separate by-products. To address these limitations, we further developed a general synthetic strategy using phosphaxanthone, which can be synthesized without using dichlorophosphine, thus allowing us to synthesize a diverse array of PORs via reaction with aryllithium compounds or aryl Grignard reagents.[43] We found that introducing an aminophenyl group at the phosphorus atom efficiently quenches fluorescence via a PET mechanism, allowing the phosphorus substituent to function as a fluorescence switch. This design enables additional functionalization at the 9-position and aminophenyl group on the phosphorus atom, exemplified by a lysosome-targeting POR probe (**23**) for visualization of endosomal maturation.

Another effective approach is to selectively label organelles chemogenetically by protein tags.[44] As an alternative approach to the development of POR-based NIR-emissive HaloTag ligands, we report the design of 1-Halo (**24**) (Figure 7B, top), featuring a 2-carboxy-benzo[*b*]thiophen-3-yl (BT) group at the 9-position of the xanthene scaffold. To introduce the HaloTag ligand to our previously developed compound (**18**), we employed post-functionalization onto the *P*-phenyl group via CuAAC, a method previously reported by our group for synthesizing compounds (**20**−**22**). Compound (**24**) was isolated as separable stereoisomers due to the restricted rotation between the xanthene framework and the BT moiety. The HaloTag ligand conjugates of the *cis* and *trans* isomers exhibited distinct staining properties in live cells (Figure 7B, bottom). Whereas the *cis* isomer showed non-specific membrane accumulation, the *trans* isomer selectively labeled HaloTag-fused proteins, enabling long-term cell division imaging. Molecular dynamics simulations indicated that differences in intermolecular hydrogen-bonding interactions cause the *cis* isomer to preferentially form membrane-associated oligomers, whereas lipid interactions suppress oligomerization of the *trans* isomer. We further applied a similar strategy to develop a series of HaloTag ligands based on NIR-emissive POR probes (**25**−**26**) by optimizing POR spirocyclization equilibrium markedly to enhance membrane permeability and accelerate cellular labeling.[45] Finally, we extended this strategy to target different organelles and sense changes in mitochondrial membrane potential and lysosomal pH through the development of *unsymmetrical* thieno-phospha-rhodamines (**27**−**30**).[46] Overall, chemogenetic strategies require careful consideration of the precise localization of protein-conjugated fluorophores relative to the lipid membrane.

4.3. Other Alternative Probes

Further validation of the molecular design strategy for super-photostable fluorophores prompted us to investigate the thiophene-containing ladder-type π-conjugated framework [1]-benzothieno[3,2-*b*][1]benzothiophene (BTBT), whose derivatives have been widely studied as organic semiconductors.[47] We anticipated that oxidation of BTBT into the corresponding thiophene-*S*,*S*-dioxide derivatives would transform this scaffold into a robust electron-accepting platform suitable for the development of super-photostable fluorophores. In addition, the aromatic character of the thiophene rings was expected to stabilize the central double bond within the BTBT framework, thereby enhancing photostability even in the absence of steric shielding by aryl substituents, in contrast to the olefinic character observed in carbon-bridged phosphole oxide-based dyes. We report the development of a series of D−π−A-type fluorescent probes (**31**−**33**), LAQ*x* (*x* = 1−3; Figure 7C), in which diphenylamine donor moieties are directly conjugated to electron-accepting BTBT skeletons containing one or two oxidized thiophene rings. These D−π−A molecules exhibit strong fluorescence in nonpolar (LDs), whereas their emission is significantly quenched in hydrophilic cytosolic environments. Among the LAQ probes, (**33**) enabled high signal-to-noise visualization of small LDs in living cells and allowed long-term time-lapse imaging of LD dynamics up to 8 days. To achieve controlled self-assembly, we introduced amino-acid−based diamides as hydrogen-bonding motifs into the (**33**) frameworks by conjugation onto the diphenylamine moiety (Figure 7D), thereby constructing lipophilic fluorophores capable of self-assembly within neutral lipids.[48] Spectroscopic and microscopic

Downloaded from pubs.acs.org/amrcda/article-pdf/7/10/1074/6859593/accountsmr.6c00184.pdf by NATL INST FOR MATLS SCIENCE (NIMS) user on 24 October 2026

https://doi.org/10.1021/accountsmr.6c00184
Acc. Mater. Res. 2026, 7, 1074−1088

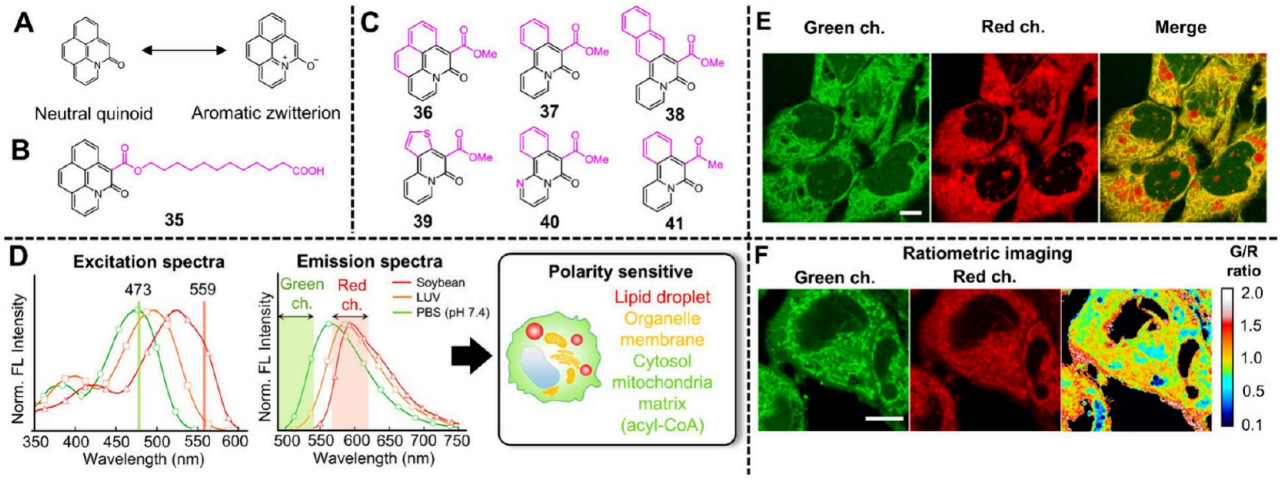


Figure 8. Representative organelle-targeting fluorescent probes for multiplex imaging and their sensing capabilities. (A) Chemical structure of a negative-solvatochromic azapyrene (AP) dye and the equilibrium between its neutral quinoid and aromatic zwitterion forms. Chemical structure of fluorescent fatty acid probe AP-C12 (**35**) (B) and arylpyridines analogue (**36-41**) (C). (D) Excitation and emission spectra of (**35**) in soybean oil, LUV lipid bilayers, and PBS (pH = 7.4, 1% DMSO). (E) Confocal images of HepG2 cells incubated with (**35**) (green channel: λ_{ex} = 473 nm and λ_{em}= 490−540 nm; red channel: λ_{ex} = 559 nm and λ_{em} = 570−620 nm). Scale bar: 10 μm. (F) Image of the G/R channel ratio for HepG2 cells incubated with (**35**). Scale bar: 10 μm. Reproduced with permission from Ref 49. Copyright 2022, Springer Nature, licensed under CC BY 4.0.

analyses revealed that a seeding strategy accelerates the transformation from a kinetically trapped monomeric state to fibrous assemblies.

5. ADVANCED MULTIPLEX ORGANELLE IMAGING

Compared with single-organelle imaging, multiplex imaging enables the simultaneous visualization of multiple subcellular organelles, providing comprehensive spatiotemporal information on organelle interactions and dynamics within living cells while reducing the number of control experiments in complex biosystems. This approach enhances the analysis of complex cellular processes while reducing cell-to-cell variability and improving imaging efficiency. Accordingly, our research is directed toward the development of multiplex imaging platforms capable of elucidating complex intracellular networks.

5.1. 3a-Azapyren-4-one: From Fatty Acid Mimics to Intelligent Fluorescent Probes

Fluorescent probes bearing molecular recognition units enable the detection of various biomolecules, while polarity-sensitive probes provide valuable information on environmental changes associated with metabolic processes. Building on our previous studies of polarity-sensitive dyes and considering the superior environmental sensitivity of 3a-azapyren-4-one (AP) (**35**), we developed a fluorescent fatty acid-mimicking probe for multiplex imaging of several organelles.[49] AP exhibits negative solvatochromism due to the equilibrium between a neutral quinoid form (Figure 8A), favored in nonpolar environments, and an aromatic zwitterionic form, stabilized in polar media. Photophysical studies of AP-Me and related derivatives (**36**−**41**) revealed that aromatic stabilization and hydrophobic shielding govern the extent of solvatochromic shifts (Figure 8B and Figure 8C). This sensitivity allows probe (**35**) to distinguish nonpolar LDs, membrane regions of intermediate polarity, and aqueous environments through distinct fluorescence emission (Figure 8D and Figure 8E). Using this approach for further ratiometric imaging (Figure 8F), we demonstrated that under the nutrient-starvation conditions, TAG degradation in hepatocytes occurs predominantly via lipolysis rather than lipophagy.

5.2. Pyrazinacene: Growing Molecular Nanoarchitecture to Unlock New Function

Our interest in further exploring the pyrazinacene system for multiplex imaging stemmed from its structural resemblance to acridine orange (AO), a fluorescent probe that remains one of the most widely used probes for RNA/DNA imaging (Supplementary Figure S2).[10,50] Both molecular frameworks possess nitrogen-rich fused aromatic cores, leading us to hypothesize that pyrazinacene derivatives might exhibit bioimaging performance analogous to those of AO (Figure 9A and Figure 9B). At the same time, this research was driven by a more fundamental question that has intrigued organic chemists for nearly a century: "*What are the consequences of linearly fusing an increasing number of pyrazine rings?*" Addressing this question requires an understanding of the historical development of azaacene chemistry. The field traces its origins to the pioneering work of Hinsberg, who reported the isolation and characterization of several oligoazatetracenes (**42**).[51] Shortly thereafter, Clar synthesized pentacene (**43**) in 1929 through the transfer dehydrogenation of 6,13-dihydropentacene with phenanthraquinone.[52,53] Although *N,N*-dihydro derivatives of larger azaacenes were prepared by Hinsberg and other early researchers, their conversion into the corresponding fully aromatic azaacenes remained a formidable synthetic challenge for several decades. This obstacle was finally overcome in 1967 by Zimmermann and Leete, whose successful oxidation of these precursors marked a turning point in azaacene chemistry. Their work not only led to the initial synthesis of a pyrazinacene (fluorubine), but also opened the door to systematic nanoarchitectonic modification of azaacene structures (**44**−**49**) and their red-shifted absorption properties. These studies stimulated further investigations that ultimately demonstrated the utility of azaacenes for organic electronic applications, as summarized in previous reviews (Table 1).[51−63]

Building upon this rich history, we became interested in investigating whether the longest pyrazinacene frameworks (λ_{abs}, max = 730 nm) could offer not only unique electronic properties but also potential utility for bioimaging, which has not been explored in the bioimaging community.[10,64] The first

https://doi.org/10.1021/accountsmr.6c00184
Acc. Mater. Res. 2026, 7, 1074−1088

Downloaded from pubs.acs.org/amrcda/article-pdf/7/10/1074/6859593/accountsmr.6c00184.pdf by NATL INST FOR MATLS SCIENCE (NIMS) user on 24 October 2026

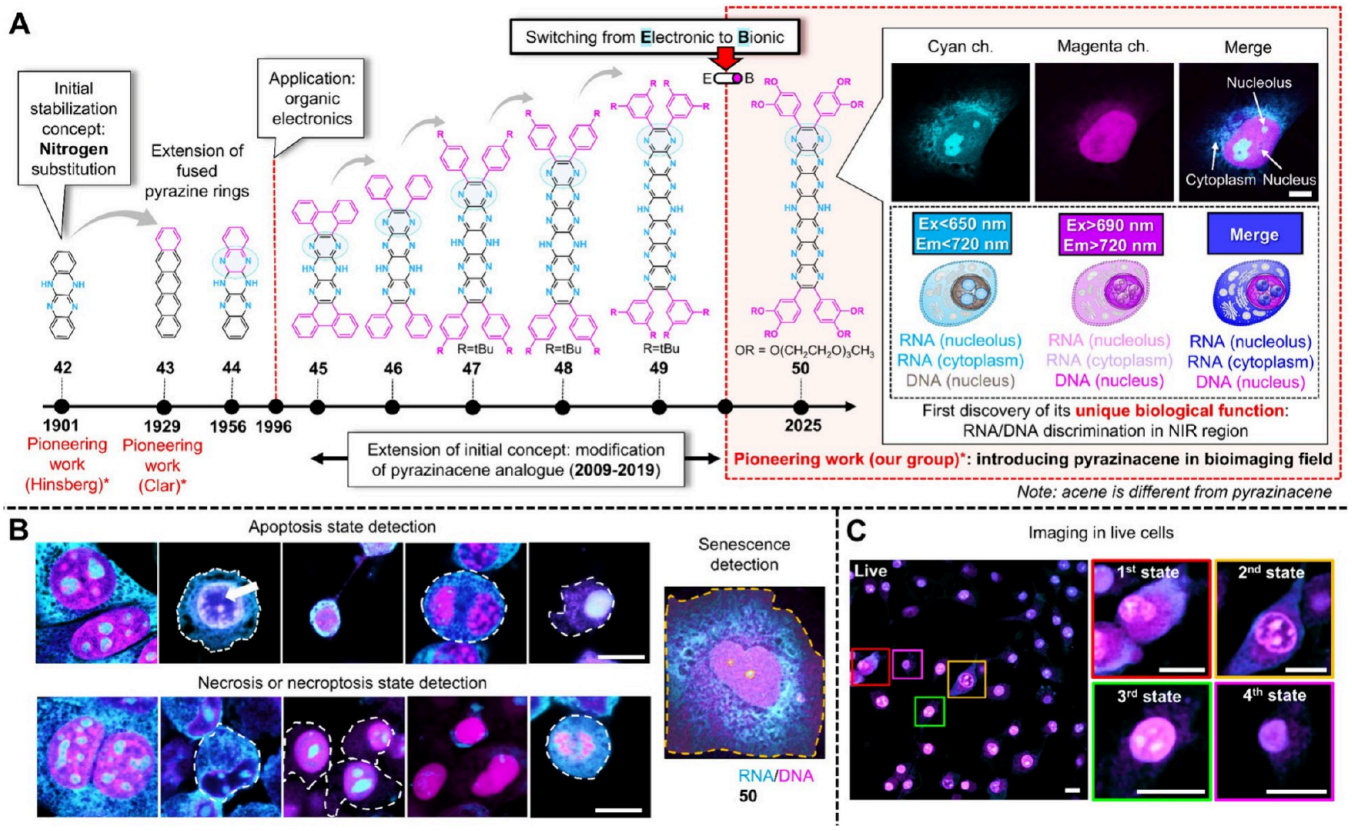


Figure 9. Historical development of pyrazinacenes. (A) Key findings of pyrazinacenes (**42**–**50**) development. Scale bar: 10 μm. (B) Detection of cell injury stages with TEG_8-N14 (**50**). Scale bar: 10 μm. (C) Representative confocal images of live HeLa cells undergoing necrosis, followed by staining with (**50**); (cyan channel: λ_{ex} = 640 nm and λ_{em} = 650–720 nm; red channel: λ_{ex} = 740 nm and λ_{em} = 750–850 nm). Scale bar: 10 μm. Reproduced with permission from Ref 64. Copyright 2025, AAAS, licensed under CC BY 4.0.

Table 1. Representative Previous Reviews Dealing with the Topic of Large Azaacenes

author	citation	title	refs
Bunz, U. H. F.	*Chem. –Eur. J.* **2009**, *15*, 6780	N-Heteroacenes	54
Bunz, U. H. F.	*Pure Appl. Chem.* **2010**, *82*, 953	The Larger N-Heteroacenes	55
Bunz, U. H. F.; et al.	*Angew. Chem. Int. Ed.* **2013**, *52*, 3810	Large N-Heteroacenes: New Tricks for Very Old Dogs?	56
Bryant, J. J.; et al.	*Chem.–Asian J.* **2013**, *8*, 1354	Click To Bind: Metal Sensors	57
Miao, Q.	*Synlett* **2012**, 326	N-Heteropentacenes and N-Heteropentacenequinones: From Molecules to Semiconductors	58
Miao, Q.	*Adv. Mater.* **2014**, *26*, 5541	Ten Years of N-Heteropentacenes as Semiconductors for Organic Thin-Film Transistors	59
Bunz, U. H. F.	*Acc. Chem. Res.* **2015**, *48*, 1676–1686	The Larger Linear N-Heteroacenes	60
Bunz, U. H. F.; et al.	*Acc. Chem. Res.* **2019**, *52*, 1575–1587	N-Heteroacenes and N-Heteroarenes as N-Nanocarbon Segments	61
Richards, G. J.; et al.	*Acc. Chem. Res.* **2021**, *54*, 3228–3240	The Pyrazinacenes	62
Freudenberg, J.; et al.	*J. Am. Chem. Soc.* **2024**, 146, 16937–16949	How to Stabilize Large Soluble (Hetero-)Acenes	63
Sutrisno, L.; et al.#	*ACS Nano* **2026**, *20*, 6493–6514	Vision of Life's Code: Molecular Probe Nanoarchitectonics for Deep RNA/DNA Illumination	50
Sutrisno, L.; et al.*	***This account***	Ladder-type π-Conjugated Heteroatom-Reinforced Nanoarchitectonics: Transformative Materials for Imaging of Cellular Components	

#Comprehensive review comparing current dual RNA/DNA imaging probes with pyrazinacene-based probes.
*Historical account tracing the development of pyrazinacene, from its initial concept to its early exploration in bioimaging field.

question that guided our early investigations of pyrazinacene was "*Where does it localize after cellular internalization?*" To investigate such pivotal question, water-soluble pyrazinacene derivative, compound (**50**), was selected from fluorophore library. Although the structural modification was minor compared with previous studies, *extensive* optimization of *bioimaging conditions* revealed its important function for the first time. Using the pyrazinacene-based probe (**50**), we achieved discrimination among multiple cellular states by detecting changes in intracellular RNA/DNA distribution via hydrogen-bonding interactions (Figure 9C). Remarkably, (**50**) selectively stained necrotic cells in live samples (Figure 8C), while following fixation enabled the detection of early senescence in UV–vis-sensitive cells (ARPE-19). Collectively,

https://doi.org/10.1021/accountsmr.6c00184
Acc. Mater. Res. 2026, 7, 1074–1088

Downloaded from pubs.acs.org/amrcda/article-pdf/7/10/1074/6859593/accountsmr.6c00184.pdf by NATL INST FOR MATLS SCIENCE (NIMS) user on 24 October 2026

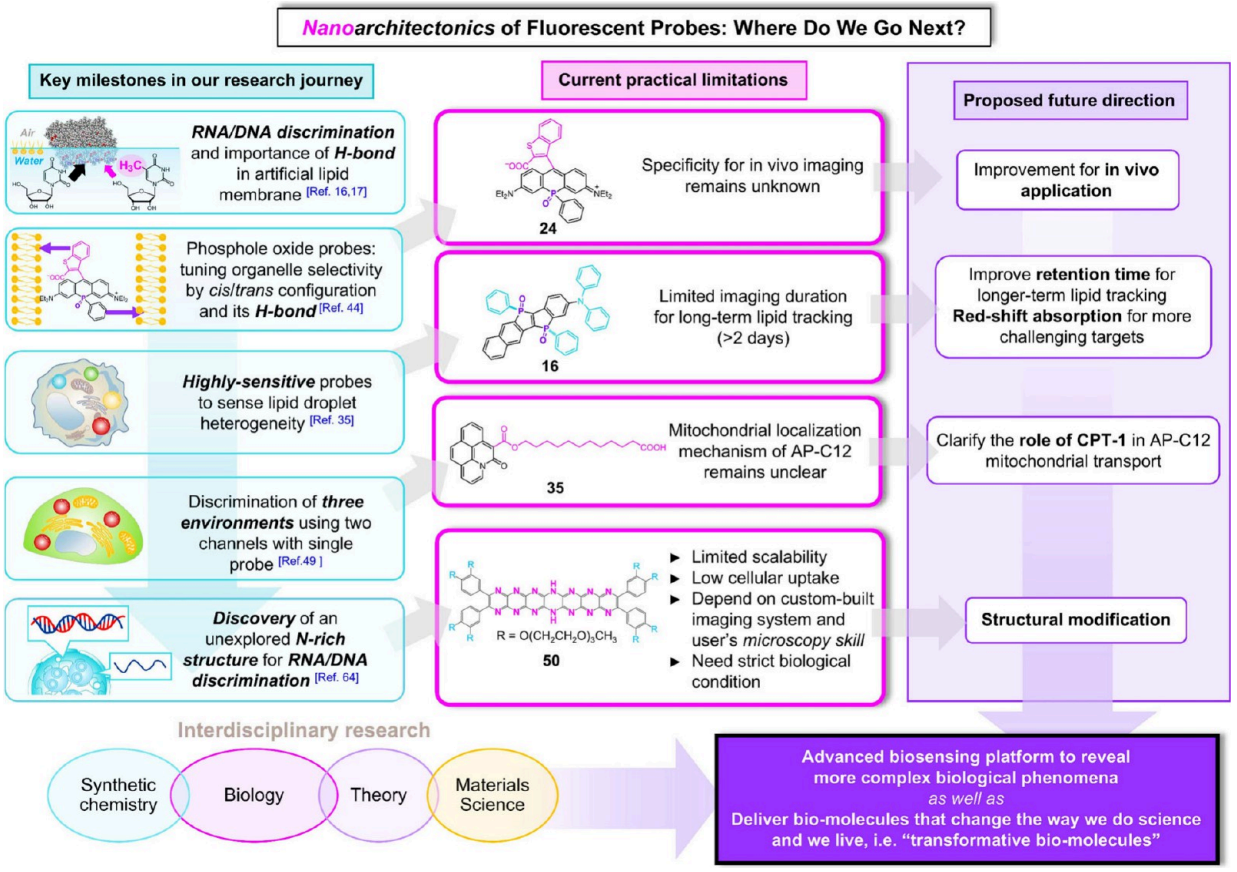


Figure 10. Summary and future outlook.

these studies demonstrate that precise engineering of pyrazinacene building blocks and careful control of their behavior can overcome current imaging limitations, enabling comprehensive visualization of single-cell fate histories without genetic manipulation or UV−vis excitation.

6. SUMMARY, CURRENT LIMITATIONS, AND FUTURE OPPORTUNITIES

An overview of the conclusions and future perspectives is presented in Figure 10, with detailed summary provided in the Supplementary Information (Supplementary Figure S2 and Supplementary Table S1−S2). Phosphole *P*-oxides offer a versatile fluorophore scaffold whose photophysical properties can be readily tuned to enhance bioimaging performance. Among phosphole-oxide fluorescent probes, we highlight our compound (**16**) functions as a polarity-sensitive probe that outperforms currently available LD dyes.[28−46] Future work integrating live-cell FLIM with single-lipid-droplet lipidomics may provide deeper insight into lipid biology.[47] Although compound (**35**) exhibits unique properties for investigating biological mechanisms, its potential requires further in-depth study. Meanwhile, our sulfur-containing lipophilic fluorophores provide a platform for programmable self-assembly in neutral lipid droplets.[48,65] Further optimization of intermolecular interactions and photophysical properties should advance sulfur-based heteroatom probes as biomarkers of intracellular self-assembly.

Most studies on the pyrazinacene structure have focused on applications in organic electronics.[50−63] In contrast, our findings highlight its untapped potential as a bioimaging probe (**50**), establishing a framework for the rational design of next-generation pyrazinacene derivatives.[64] As this study represents the first demonstration of their bioimaging application, further structure optimization is needed to overcome their aggregation behavior for long-term imaging, which potentially interfere with organelle function.

Collectively, our studies demonstrate that rational molecular engineering of bioimaging probes can drive biological discovery.[66−68] Such systems exemplify *nanoarchitectonics*, in which chemical building blocks and biological functions are integrated to reveal complex biological phenomena.[8−12] Our personal vision of the field is to shift focus beyond *"What fluorophores can we make?"* toward ***"What fluorophores should we make to answer remaining uncovered biological questions?"***. Finally, we hope this Account will stimulate interdisciplinary research integrating state-of-the-art chemistry, biology, theoretical science, and nanoarchitectonics to advance our understanding of mysterious biological systems.

■ ASSOCIATED CONTENT

Supporting Information

The Supporting Information is available free of charge at https://pubs.acs.org/doi/10.1021/accountsmr.6c00184.

Representative example of molecular design of probes discussed in this Account, selected examples of existing chemical probes for simultaneous RNA and DNA visualization, chemical structures of the existing compounds plotted according to their excitation wavelengths, comparison of current compounds for dual RNA/DNA imaging, summary of selected examples of photophysical

https://doi.org/10.1021/accountsmr.6c00184
Acc. Mater. Res. 2026, 7, 1074−1088

Downloaded from pubs.acs.org/amrcda/article-pdf/7/10/1074/6859593/accountsmr.6c00184.pdf by NATL INST FOR MATLS SCIENCE (NIMS) user on 24 October 2026

properties of chemical probes developed from our group for ion sensing, summary of selected photophysical properties of chemical probes developed by our group based on phosphorus-heteroatom reinforcement (PDF)

AUTHOR INFORMATION

Corresponding Authors

Katsuhiko Ariga − *Research Center for Materials Nanoarchitectonics (MANA), NIMS, Tsukuba, Ibaraki 305-0044, Japan; Graduate School of Frontier Sciences, The University of Tokyo, Kashiwa 277-8561, Japan;* orcid.org/0000-0002-2445-2955; Email: ARIGA.Katsuhiko@nims.go.jp

Shigehiro Yamaguchi − *Institute of Transformative Bio-Molecules (WPI-ITbM), Nagoya University, Chikusa 464-8601, Japan; Department of Chemistry, Graduate School of Science and Integrated Research Consortium on Chemical Science (IRCCS), Nagoya University, Nagoya 464-8602, Japan;* orcid.org/0000-0003-0072-8969; Email: yamaguchi@chem.nagoya-u.ac.jp

Authors

Linawati Sutrisno − *State Key Laboratory of Radiation Medicine and Protection, School of Radiation Medicine and Protection, Collaborative Innovation Center of Radiological Medicine of Jiangsu Higher Education Institutions, Soochow University, Suzhou 215123, PR China; International Center for Young Scientists (ICYS), National Institute for Materials Science (NIMS), Tsukuba, Ibaraki 305-0044, Japan;* orcid.org/0000-0003-3085-9660

Masayasu Taki − *Institute for Glyco-core Research (iGCORE), Gifu University, Gifu 501-1193, Japan;* orcid.org/0000-0003-2185-4593

Complete contact information is available at: https://pubs.acs.org/10.1021/accountsmr.6c00184

Author Contributions

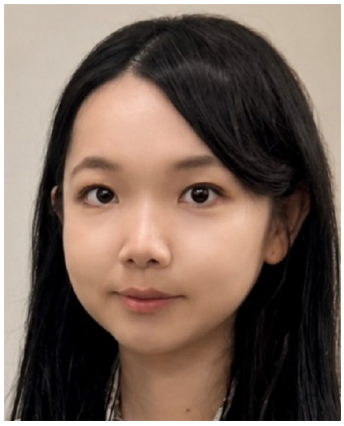
L.S. planned the manuscript, prepared the figure, researched the literature, and wrote original draft. S.Y. edited the manuscript. L.S. and M.T. prepared the chemical structure. L.S., M.T., K.A. and S.Y. discussed and revised the manuscript. All authors have approved the final version of the manuscript.

Notes

The authors used artificial intelligence tools solely to improve the readability of the manuscript. All content was outlined, reviewed, and approved by the authors, who take full responsibility for the accuracy, integrity, and final content of the manuscript.

The authors declare no competing financial interest.

Biographies



Linawati Sutrisno is currently an Associate Professor at Soochow University. She earned her Ph.D. from the University of Tsukuba and postdoctoral training (Professor Katsuhiko Ariga's group), supported by NIMS and Japan Society for the Promotion of Science (JSPS). In 2024, she started her independent career as an ICYS Researcher at NIMS (joint with Professor Masayasu Taki). Her research focuses on bioimaging, cancer to tissue regeneration.



Masayasu Taki is currently a Professor at Gifu University. He obtained his Ph.D. from Osaka University and conducted postdoctoral research as a JSPS research fellow at Northwestern University. In 2004, he was appointed as an Assistant Professor at Kyoto University and further joined the WPI-ITbM at Nagoya University as a Designated Associate Professor in Professor Shigehiro Yamaguchi's group. His research field is chemical biology, with a particular focus on the rational design of fluorescent probes for bioimaging.



Katsuhiko Ariga is currently a group leader of the Supermolecules Group and a Senior Scientist with Special Missions of Research Center

Downloaded from pubs.acs.org/amrcda/article-pdf/7/10/1074/6859593/accountsmr.6c00184.pdf by NATL INST FOR MATLS SCIENCE (NIMS) user on 24 October 2026

https://doi.org/10.1021/accountsmr.6c00184
Acc. Mater. Res. 2026, 7, 1074−1088

for MANA. He is also appointed as a Professor at The University of Tokyo. He received his Ph.D. degree from the Tokyo Institute of Technology in 1990. His expertise is in supramolecular chemistry and material nanoarchitectonics.



Shigehiro Yamaguchi is a Professor at Nagoya University and Vice Director of WPI-ITbM. He received his Ph.D. from Kyoto University in 1997 and served as an Assistant Professor in Professor Kohei Tamao's group, including a period as a visiting scholar with Professor Timothy M. Swager at MIT. His research focuses on main-group chemistry-based functional materials and fluorescent probes for bioimaging.

■ ACKNOWLEDGMENTS

The authors would like to express their sincere gratitude to all collaborators engaged in the research described in this Account. This work was supported in part by the Japan Society for the Promotion of Science (JSPS) KAKENHI Grant Numbers, 25K23571 and 26K15594 to L.S., 26K01643 to M.T, 23H05459 and 25H00898 to K.A, 22K21346 and 25H01261 as well as by JST CREST (JRMJCR21O5) to S.Y. The authors would acknowledge support by Suzhou Fundamental Research Project (SJC2023001).

■ REFERENCES

(1) Koo, K.; Tripathy, P.; Kenny, S.E.; Farhana, F.Z.; Shiddiky, M. J. A. Controlling nucleic acid affinity interactions and adsorption dynamics on electrode material surfaces for biosensing applications. *Acc. Mater. Res.* **2026**, *7*, 431−445.
(2) Wang, Z.; Zhao, Y.; Zhang, Y.-B. The future of reticular chemistry: from structural discovery to programmable matter and artificial intelligence. *Acc. Mater. Res.* **2026**, *7*, 425−430.
(3) Oviedo, F.; Ferres, J.L.; Buonassisi, T.; Butler, K.T. Interpretable and explainable machine learning for materials science and chemistry. *Acc. Mater. Res.* **2022**, *3*, 597−607.
(4) Liu, Q.; Braunstein, P.; Lang, J.P. Photoresponsive coordination polymer single crystal platforms: design and applications. *Acc. Mater. Res.* **2025**, *6*, 183−194.
(5) Wang, Z.; Kenry. Cellular morphometry for interrogating nanomaterial−cell interactions. *Acc. Mater. Res.* **2026**, *7*, 777−788.
(6) Yan, C.; Zhu, Z.; Yao, Y.; Wang, Q.; Guo, Z.; Zhu, W.H. Engineering near-infrared fluorescent probes based on modulation of molecular excited states. *Acc. Mater. Res.* **2024**, *5*, 64−75.
(7) Huang, Z.; Wang, D.; Zhang, Q.; Zhang, Y.; Peng, R.; Tan, W. Leveraging aptamer-based DNA nanotechnology for bioanalysis and cancer therapeutics. *Acc. Mater. Res.* **2024**, *5*, 438−452.
(8) Ariga, K. Nanoarchitectonics: the method for everything in materials science. *Bull. Chem. Soc. Jpn.* **2024**, *97*, No. uoad001.
(9) Ariga, K. Materials Nanoarchitectonics: collaboration between chem, nano and mat. *ChemNanoMat* **2023**, *9*, No. e202300120.
(10) Sutrisno, L.; Sun, K.; Ariga, K. Vision of life's code: molecular probe nanoarchitectonics for deep RNA/DNA illumination. *ACS Nano* **2026**, *20*, 6493−6514.
(11) Ariga, K. Langmuir−blodgett nanoarchitectonics, out of the box. *Acc. Mater. Res.* **2022**, *3*, 404−410.
(12) Komiyama, M.; Yoshimoto, K.; Sisido, M.; Ariga, K. Chemistry can make strict and fuzzy controls for bio-systems: DNA nano-architectonics and cell-macromolecular nanoarchitectonics. *Bull. Chem. Soc. Jpn.* **2017**, *90*, 967−1004.
(13) Ariga, K.; Mori, T.; Hill, J.P. Mechanical control of nanomaterials and nanosystems. *Adv. Mater.* **2012**, *24*, 158−176.
(14) Hirai, M.; Tanaka, N.; Sakai, M.; Yamaguchi, S. Structurally constrained boron-, nitrogen-, silicon-, and phosphorus-centered polycyclic π-conjugated systems. *Chem. Rev.* **2019**, *119*, 8291−8331.
(15) Yamaguchi, S.; Fukazawa, A.; Taki, M. Phosphole p-oxide-containing π-electron materials: synthesis and applications in fluorescence imaging. *J. Synth. Org. Chem., Jpn.* **2017**, *75*, 1179−1187.
(16) Ariga, K.; Kunitake, T. Molecular recognition at air−water and related interfaces: complementary hydrogen bonding and multisite interaction. *Acc. Chem. Res.* **1998**, *31*, 371−378.
(17) Mori, T.; Okamoto, K.; Endo, H.; Hill, J.P.; Shinoda, S.; Matsukura, M.; Tsukube, H.; Suzuki, Y.; Kanekiyo, Y.; Ariga, K. Mechanical tuning of molecular recognition to discriminate the single-methyl-group difference between thymine and uracil. *J. Am. Chem. Soc.* **2010**, *132*, 12868−12870.
(18) Sakakibara, K.; Joyce, L. A.; Mori, T.; Fujisawa, T.; Shabbir, S. H.; Hill, J. P.; Anslyn, E. V.; Ariga, K. A mechanically controlled indicator displacement assay. *Angew. Chem. Int. Ed.* **2012**, *51*, 9643−9646.
(19) Fukazawa, A.; Osaki, H.; Yamaguchi, S. Hydroxyphenyl-substituted benzophosphole oxides: impact of the intramolecular hydrogen bond on the fluorescence properties. *Asian J. Org. Chem.* **2014**, *3*, 122−127.
(20) Taki, M.; Wolford, J.L.; O'Halloran, T.V. Emission ratiometric imaging of intracellular zinc: design of a benzoxazole fluorescent sensor and its application in two-photon microscopy. *J. Am. Chem. Soc.* **2004**, *126*, 712−713.
(21) Taki, M.; Watanabe, Y.; Yamamoto, Y. Development of ratiometric fluorescent probe for zinc ion based on indole fluorophore. *Tetrahedron Lett.* **2009**, *50*, 1345−1347.
(22) Taki, M.; Desaki, M.; Ojida, A.; Iyoshi, S.; Hirayama, T.; Hamachi, I.; Yamamoto, Y. Fluorescence imaging of intracellular cadmium using a dual-excitation ratiometric chemosensor. *J. Am. Chem. Soc.* **2008**, *130*, 12564−12565.
(23) Taki, M.; Iyoshi, S.; Ojida, A.; Hamachi, I.; Yamamoto, Y. Development of highly sensitive fluorescent probes for detection of intracellular copper(I) in living systems. *J. Am. Chem. Soc.* **2010**, *132*, 5938−5939.
(24) Taki, M.; Akaoka, K.; Mitsui, K.; Yamamoto, Y. A mitochondria-targeted turn-on fluorescent probe based on a rhodol platform for the detection of copper(I). *Org. Biomol. Chem.* **2014**, *12*, 4999.
(25) Taki, M.; Akaoka, K.; Iyoshi, S.; Yamamoto, Y. Rosamine-based fluorescent sensor with femtomolar affinity for the reversible detection of a mercury ion. *Inorg. Chem.* **2012**, *51*, 13075−13077.
(26) Taki, M.; Asahi, F.; Hirayama, T.; Yamamoto, Y. Design and synthesis of fluorescent probe for polyhistidine tag using macrocyclic nickel (II) complex and fluorescein conjugate. *Bull. Chem. Soc. Jpn.* **2011**, *84*, 386−394.
(27) Yamaguchi, E.; Wang, C.; Fukazawa, A.; Taki, M.; Sato, Y.; Sasaki, T.; Ueda, M.; Sasaki, N.; Higashiyama, T.; Yamaguchi, S. Environment-sensitive fluorescent probe: a benzophosphole oxide with an electron-donating substituent. *Angew. Chem. Int. Ed.* **2015**, *54*, 4539−4543.
(28) Taki, M.; Ogasawara, H.; Osaki, H.; Fukazawa, A.; Sato, Y.; Ogasawara, K.; Higashiyama, T.; Yamaguchi, S. A red-emitting ratiometric fluorescent probe based on a benzophosphole P-oxide scaffold for the detection of intracellular sodium ion. *Chem. Commun.* **2015**, *51*, 11880−11883.
(29) Ogasawara, H.; Grzybowski, M.; Hosokawa, R.; Sato, Y.; Taki, M.; Yamaguchi, S. A far-red fluorescent probe based on a phospha-

Downloaded from pubs.acs.org/amrcda/article-pdf/7/10/1074/6859593/accountsmr.6c00184.pdf by NATL INST FOR MATLS SCIENCE (NIMS) user on 24 October 2026

fluorescein scaffold for cytosolic calcium imaging. *Chem. Commun.* **2018**, *54*, 299−302.
(30) Wang, C.; Fukazawa, A.; Taki, M.; Sato, Y.; Higashiyama, T.; Yamaguchi, S. A phosphole oxide based fluorescent dye with exceptional resistance to photobleaching: a practical tool for continuous imaging in STED microscopy. *Angew. Chem. Int. Ed.* **2015**, *54*, 15213−15217.
(31) Wang, C.; Taki, M.; Sato, Y.; Fukazawa, A.; Higashiyama, T.; Yamaguchi, S. Super-photostable phosphole-based dye for multiple-acquisition stimulated emission depletion imaging. *J. Am. Chem. Soc.* **2017**, *139*, 10374−10381.
(32) Wang, C.; Taki, M.; Sato, Y.; Tamura, Y.; Yaginuma, H.; Okada, Y.; Yamaguchi, S. A photostable fluorescent marker for the super-resolution live imaging of the dynamic structure of the mitochondrial cristae. *Proc. Natl. Acad. Sci. U.S.A.* **2019**, *116*, 15817−15822.
(33) Wang, C.; Taki, M.; Kajiwara, K.; Wang, J.; Yamaguchi, S. Phosphole-oxide-based fluorescent probe for super-resolution stimulated emission depletion live imaging of the lysosome membrane. *ACS Mater. Lett.* **2020**, *2*, 705−711.
(34) Wang, J.; Taki, M.; Ohba, Y.; Arita, M.; Yamaguchi, S. Fluorescence lifetime imaging of lipid heterogeneity in the inner mitochondrial membrane with a super-photostable environment-sensitive probe. *Angew. Chem. Int. Ed.* **2024**, *63*, No. e202404328.
(35) Wang, J.; Kajiwara, K.; Kesherwani, M.; Tama, F.; Ohsaki, Y.; Yamaguchi, S.; Taki, M. Single-cell fluorescence analysis of lipid droplet compositional dynamics during triacylglycerol catabolism. *J. Am. Chem. Soc.* **2025**, *147*, 41514−41523.
(36) Fukazawa, A.; Suda, S.; Taki, M.; Yamaguchi, E.; Grzybowski, M.; Sato, Y.; Higashiyama, T.; Yamaguchi, S. Phospha-fluorescein: a red-emissive fluorescein analogue with high photobleaching resistance. *Chem. Commun.* **2016**, *52*, 1120−1123.
(37) Grzybowski, M.; Taki, M.; Yamaguchi, S. Selective conversion of P=O-bridged rhodamines into P=O rhodols: solvatochromic near-infrared fluorophores. *Chem. −Eur. J.* **2017**, *23*, 13028−13032.
(38) Grzybowski, G.; Taki, M.; Senda, K.; Sato, Y.; Ariyoshi, T.; Okada, Y.; Kawakami, R.; Imamura, T.; Yamaguchi, S. A highly photostable near-infrared labeling agent based on a phospha-rhodamine for long-term and deep imaging. *Angew. Chem. Int. Ed.* **2018**, *57*, 10137−10141.
(39) Grzybowski, M.; Taki, M.; Kajiwara, K.; Yamaguchi, S. Effects of amino group substitution on the photophysical properties and stability of near-infrared fluorescent P-rhodamines. *Chem. −Eur. J.* **2020**, *26*, 7912−7917.
(40) Chai, X. Y.; Cui, X. Y.; Wang, B. G.; Yang, F.; Cai, Y.; Wu, Q. Y.; Wang, T. Near-infrared phosphorus-substituted rhodamine with emission wavelength above 700 nm for bioimaging. *Chem. −Eur. J.* **2015**, *21*, No. 16754.
(41) Zhou, X. Q.; Lai, R.; Beck, J. R.; Li, H.; Stains, C. I. Chemoselective alteration of fluorophore scaffolds as a strategy for the development of ratiometric chemodosimeters. *Chem. Commun.* **2016**, *52*, No. 12290.
(42) Ogasawara, H.; Tanaka, Y.; Taki, M.; Yamaguchi, S. Late-stage functionalisation of alkyne-modified phospha-xanthene dyes: lysosomal imaging using an off−on−off type of pH probe. *Chem. Sci.* **2021**, *12*, 7902−7907.
(43) Asada, Y.; Taki, M.; Yamaguchi, S. Synthetic strategy for multi-functionalized phospharhodamines via catalytic P-arylation. *Bull. Chem. Soc. Jpn.* **2023**, *96*, 601−606.
(44) Wu, Q.; Taki, M.; Tanaka, Y.; Kesherwani, M.; Phung, Q.M.; Enoki, S.; Okada, Y.; Tama, F.; Yamaguchi, S. Stereochemistry-dependent labeling of organelles with a near-infrared-emissive phosphorus-bridged rhodamine dye in live-cell imaging. *Angew. Chem. Int. Ed.* **2024**, *63*, No. e202400711.
(45) Tanaka, Y.; Taki, M.; Yamaguchi, S. Near-infrared fluorescent HaloTag ligands for efficient organelle labelling in live cells. *Chem. Commun.* **2025**, *61*, 1164.
(46) Ma, S.; Asada, Y.; Yamaguchi, S.; Taki, M. Unsymmetric thieno-phospha-rhodamines: a new class of near-infrared fluorescent probes for stimuli-responsive organelle imaging. *Chem. Commun.* **2025**, *61*, No. 14653.
(47) Taki, M.; Kajiwara, K.; Yamaguchi, E.; Sato, Y.; Yamaguchi, S. Fused thiophene-S, S-dioxide-based super-photostable fluorescent marker for lipid droplets. *ACS Mater. Lett.* **2021**, *3*, 42−49.
(48) Naruse, M.; Ogi, S.; Kajiwara, K.; Fukaya, N.; Sato, Y.; Taki, M.; Yamaguchi, S. Kinetically controlled self-assembly of a lipophilic fluorophore with phenylalanine-based diamides in artificial lipid droplets. *Small* **2026**, *22*, No. e13411.
(49) Kajiwara, K.; Osaki, H.; Greßies, S.; Kuwata, K.; Kim, J.H.; Gensch, T.; Sato, Y.; Glorius, F.; Yamaguchi, S.; Taki, M. A negative-solvatochromic fluorescent probe for visualizing intracellular distributions of fatty acid metabolites. *Nat. Commun.* **2022**, *13*, 2533.
(50) Byvaltsev, V. A.; Bardonova, L. A.; Onaka, N. R.; Polkin, R. A.; Ochkal, S. V.; Shepelev, V. V.; Aliyev, M. A.; Potapov, A. A. Acridine orange: A Review of Novel Applications for Surgical Cancer Imaging and Therapy. *Front. Oncol.* **2019**, *9*, 925.
(51) Hinsberg, O. Multi-level nitrogenous ring systems liebigs. *Ann. Chem.* **1901**, *319*, 257−286.
(52) Clar, E.; John, Fr Polynuclear aromatic hydrocarbons and their derivatives. V. Naphthoanthracenes, their oxidation products and a new class of deeply colored hydrocarbons. *Ber. Dtsch. Chem. Ges. B* **1929**, *62*, 3021−3029.
(53) Miao, S.; Brombosz, S. M.; Schleyer, P. v. R.; Wu, J. I.; Barlow, S.; Marder, S. R.; Hardcastle, K. I.; Bunz, U. H. F. Are *N,N*-dihydrodiazatetracene derivatives antiaromatic? *J. Am. Chem. Soc.* **2008**, *130*, 7339−7344.
(54) Bunz, U. H. F. N-heteroacenes. *Chem. −Eur. J.* **2009**, *15*, 6780.
(55) Bunz, U. H. F. The larger N-heteroacenes. *Pure Appl. Chem.* **2010**, *82*, 953.
(56) Bunz, U. H. F.; Engelhart, D. C. J. U.; Lindner, D. C. B. D.; Schaffroth, M. S. M. Large N-heteroacenes: new tricks for very old dogs? *Angew. Chem. Int. Ed.* **2013**, *52*, 3810.
(57) Bryant, J. J.; Bunz, U. H. F. Click to bind: metal sensors. *Chem.−Asian J.* **2013**, *8*, 1354.
(58) Miao, Q. N-heteropentacenes and N-heteropentacenequinones: from molecules to semiconductors. *Synlett* **2012**, *23*, 326−336.
(59) Miao, Q. Ten years of N-heteropentacenes as semiconductors for organic thin-Film transistors. *Adv. Mater.* **2014**, *26*, 5541.
(60) Bunz, U. H. F. The larger linear N-heteroacenes. *Acc. Chem. Res.* **2015**, *48*, 1676−1686.
(61) Bunz, U. H. F.; Freudenberg, J. N-Heteroacenes and N-Heteroarenes as N-Nanocarbon segments. *Acc. Chem. Res.* **2019**, *52*, 1575−1587.
(62) Richards, G.J.; Hill, J.P. The pyrazinacenes. *Acc. Chem. Res.* **2021**, *54*, 3228−3240.
(63) Bunz, U. H. F.; Freudenberg, J. How to stabilize large soluble (hetero-)acenes. *J. Am. Chem. Soc.* **2024**, *146*, 16937−16949.
(64) Sutrisno, L.; Richards, G. J.; Evans, J. D.; Matsumoto, M.; Li, X.; Uto, K.; Hill, J. P.; Taki, M.; Yamaguchi, S.; Ariga, K. Visualizing the chronicle of multiple cell fates using a near-IR dual-RNA/DNA−targeting probe. *Sci. Adv.* **2025**, *11*, No. eadz6633.
(65) Naruse, M.; Fukaya, N.; Imai, Y.; Ogi, S.; Taki, M.; Yamaguchi, S. Programmable Construction of Supramolecular Polymers Achieved in Neutral Lipid Environments. *Nat. Commun.* **2026**, *17*, 5732.
(66) Ohashi, T.; Sutrisno, L.; Yamashita, Yu; Ariga, K. Biochemical pathways for device nanoarchitectonics: organic semiconductors interfaced with biomolecular systems. *Appl. Phys. Express.* **2026**, *19*, No. 040106.
(67) Sutrisno, L.; Ariga, K. Pore-engineered nanoarchitectonics for cancer therapy. *NPG Asia Mater.* **2023**, *15*, 21.
(68) Sutrisno, L.; Chen, H.; Chen, Y.; Yoshitomi, T.; Kawazoe, N.; Yang, Y.; Chen, G. Composite scaffolds of black phosphorus nanosheets and gelatin with controlled pore structures for photothermal cancer therapy and adipose tissue engineering. *Biomaterials.* **2021**, *275*, No. 120923.

Downloaded from pubs.acs.org/amrcda/article-pdf/7/10/1074/6859593/accountsmr.6c00184.pdf by NATL INST FOR MATLS SCIENCE (NIMS) user on 24 October 2026

https://doi.org/10.1021/accountsmr.6c00184
Acc. Mater. Res. 2026, 7, 1074−1088